

A new method for flow-based network intrusion detection using inverse statistical physics

Camila Pontes, João Gondim, Matt Bishop and Marcelo Marotta

Abstract—Network Intrusion Detection Systems (NIDS) play an important role as tools for identifying potential network threats. In the context of ever-increasing traffic volume on computer networks, flow-based NIDS arise as good solutions for real-time traffic classification. In recent years, different flow-based classifiers have been proposed based on both shallow and deep learning. Nevertheless, these classical machine learning algorithms have some limitations. For instance, they require large amounts of labeled data, which might be difficult to obtain. Additionally, most machine learning models are not general enough to be applied in different contexts. To overcome these limitations, we propose a new flow-based classifier, called Energy-based Flow Classifier (EFC). This anomaly-based classifier uses inverse statistics to infer a model based on labeled benign examples. We show that EFC is capable to accurately perform a two-class flow classification and is resilient to context change. Given the positive results obtained, we consider EFC to be a promising algorithm to perform flow-based traffic classification.

Index Terms—Flow-based Network Intrusion Detection, Anomaly-based Network Intrusion Detection, Network Flow Classification, Network Intrusion Detection Systems, Energy-based Flow Classifier.

I. INTRODUCTION

SYMANTEC'S Internet Security Threat Report [1] points out a 56% increase in the number of web attacks in 2019. Network scans, denial of service, and brute force attacks are among the most common threats. Such malicious activities threaten not only individuals, but also some collective organizations such as public health, financial, and government institutions. In this context, Network Intrusion Detection Systems (NIDSs) play an important role as tools for identifying potential threats.

There are two different approaches for NIDSs regarding the kind of data analyzed: packet-based and flow-based. In the former, deep packet inspection is performed taking into account individual packet payloads as well as header information. In the latter, flows, as packet collections, are analyzed regarding their properties, *e.g.*, duration, number of packets, number of bytes, and source/destination port. In order to perform traffic classification in real time, a huge volume of data must be analyzed preventing more accurate and complex mechanisms to be used, such as deep packet inspection. Since flow-based approaches can classify the whole traffic inspecting an equivalent to 0.1% of the total volume [2], NIDSs based

on flow analysis arise as good solutions for real-time traffic classification.

In recent years, different flow-based classifiers have been proposed based on both shallow and deep learning [3]. According to the report in [3], the best flow-based classifiers achieve around 99% accuracy. Although quite accurate, classical Machine Learning (ML) based classifiers require labeled malicious traffic samples to perform training. However, real traffic samples might be difficult to label as malicious. ML based classifiers training process, in turn, is specific for the context considered making them unable to be easily generalized. Moreover, ML algorithms are well-known to be black box mechanisms difficult to be readjusted in detail. In this regard, there is a clear need of a new flow-based classifier for NIDSs able to be readjusted in details (*i.e.*, white box) without training, based on malicious examples, and resilient to context change.

We propose a new flow-based classifier called Energy-based Flow Classifier (EFC). EFC is an anomaly-based classifier, *i.e.*, it learns from labeled data characteristics typical of normal traffic and use this information to classify unlabeled flows. In this process, flow features are analyzed, both individually and jointly, to identify frequent values associated to normal traffic behavior. Feature values which seldom occur are, in turn, regarded as abnormal. This procedure, as described, resembles problems involving energy landscapes in statistical physics, where the energy of a given system state is determined by the configuration assumed by each individual particle in the system. Particles on lower energy configurations are more frequent and tend to be present in a system in "normal" state. Following this analogy, each specific single or joint flow feature occurrence contribute to raise or lower the "energy" of a given flow. So, a certain "energy" value may be associated with each unlabeled flow and compared to a given normality threshold. Therefore, the idea and rationale rely on mapping network flow anomaly detection to a similar problem already successfully addressed by statistical physics. This is the motivation that drives the method supporting EFC.

EFC is a white box flow classifier based on inverse statistical physics. Since EFC is based on a multivariate statistical model, it can be analyzed in detail regarding individual parameter values. Moreover, as long as normal traffic can be characterized in flows, EFC will be able to detect the opposite, *i.e.*, malicious traffic. We compared the performance of EFC against a variety of classifiers trained within different scenarios, *i.e.*, a simulated and a real network from the flow dataset CIDDs-001 [4]. Our results show that classifiers based on shallow and deep learning are highly sensitive to context change. Meanwhile, EFC was

C. Pontes, J. Gondim and M. A. Marotta are with the University of Brasilia, Brazil, emails: cftpontes@gmail.com, gondim@unb.br, marcelo.marotta@unb.br;

M. Bishop is with the University of California at Davis, Davis, USA, email: mabishop@ucdavis.edu

the only classifier to achieve high accuracy when subjected to context change regarding the two different scenarios from the dataset. Our main contributions are as follows:

- The mapping of flow features to serve as input for an inverse statistical physics based model.
- The proposal of a flow classifier for NIDSs based on inverse statistical physics.
- A comparison among EFC and the best classifiers found on the literature of flow-based NIDSs.

The rest of this article is structured as follows. In Section II, we briefly present the state-of-the-art in flow-based NIDSs. In Section III, we describe the structure of a network flow and present a preliminary analysis of the flow dataset used here. In Section IV, we introduce the statistical model proposed and the classifier implementation. In Section V, we present results obtained regarding the analysis of the statistical model and the classification experiments performed. Finally, in Section VI, we present our conclusions and future work.

II. RELATED WORK

In this section, we briefly review the state-of-the-art in flow-based network intrusion detection. We show some early work in the field, as well as the recent advances. In the end, some previous work performed on CIDDs-001 dataset are shown.

In 2011, Winter *et al.* [5] presented an innovative approach for flow-based network traffic classification. They propose a classifier that uses a one-class Support Vector Machine (SVM) with learning based on malicious traffic examples. Their algorithm achieves around 98% accuracy with a very low false positive rate. We revisit this idea proposing a new one-class classifier with training, however, based solely on benign traffic examples instead of malicious ones.

Apart from one-class-based approaches, which are not easily found in literature, several ML-based and statistical-based flow classifiers were proposed in recent years. In 2017, Umer *et al.* wrote a comprehensive survey on flow-based NIDSs [3], in which all recently proposed flow-based classifiers were reviewed. In this work, we deploy most of the ML-classifiers covered in [3] to serve as baselines, against which we compare our classifier.

Recently, flow-based intrusion detection has been explored in modern contexts, *i.e.*, Internet of Things (IoT) networks [6], [7] and cloud environments [8], [9]. The proposed solutions for intrusion detection in IoT and cloud environments achieved satisfactory classification accuracy and feasible running times. However, their capability to be reused in different scenarios without retraining is still a matter of investigation. In fact, most of the proposed solutions from literature assume that there will be available training sets to be used in all contexts, which is not necessarily true. In this regard, we propose a flow-classifier solution able to be adapted to different contexts without retraining.

To assess EFC performance, we selected a network flow dataset: CIDDs-001. This dataset was used by Verma and Ranga [10] to assess the performance of k-nearest neighbours (KNN) and k-means clustering algorithms when classifying traffic. Both algorithms achieved over 99% accuracy. Also,

Ring *et al.* [11] explored slow port scans detection using CIDDs-001. The approach proposed by them is capable of accurately recognizing the attacks with low false alarm rate. Finally, Abdulhammed *et al.* [12] also performed flow-based classification on CIDDs-001, and proposed an approach that is robust considering imbalanced network traffic. In summary CIDDs-001 is an up-to-date and relevant dataset to be used for network flow-classification solutions, being our dataset choice for assessing the performance of EFC.

III. PRELIMINARIES

For a given network flow to be considered malicious, it must present at least one observable abnormality. In other words, from the perspective of an anomaly-based classifier, a combination of anomalies is what characterizes a malicious flow. In this regard, as a preliminary analysis, we are going to characterize flows considering two distinct classes, *i.e.*, normal and malicious. If it is observed that flows labeled as malicious present abnormal characteristics, as expected, then EFC must be able to correctly classify unlabeled flows after learning normal traffic characteristics. As it will be later seen, learning here corresponds to deriving a model for normal traffic from normal traffic characteristics. Therefore, next we analyze network flows regarding their features. We also describe the statistical distribution of flows within CIDDs-001. And finally, we investigate if there is significant feature variation between different labeled flow classes to consider them malicious or normal.

A. Network flow profiling

A network flow is a set of packets that traverses intermediary nodes between end points within a given time interval. Under the perspective of an intermediary node, *i.e.*, an observation point, all packets belonging to a given flow have a set of common features called flow keys. It means that flow keys do not change for packets belonging to the same flow, while the remaining features might vary. FlowScan [13] is an example of tool capable of collecting data from a set of packets and extracting flow features to be later exported in different formats, such as NetFlow and IPFIX. Since NetFlow is the most commonly used format, its main features are listed below:

- Source/Destination IP (flow key) - determine the origin and destination of a given flow in the network;
- Source/Destination port (flow key) - characterize different kinds of network services *e.g.*, port 22 is used to access an ssh service;
- Protocol (flow key) - characterizes flows regarding the transport protocol used *e.g.*, TCP, UDP, ICMP.
- Number of packets (feature) - total number of packets captured in a flow;
- Number of bytes (feature) - total number of bytes in a flow;
- Duration (feature) - total duration of a flow in seconds;
- Initial timestamp (feature) - system time when a flow started to be captured;

Other features such as TCP Flags and Type of Service might also be exported in some cases. The combination of different flow keys and features characterize a flow and determine its particular behavior.

It is important to note that individual packets usually have more features than a flow. The number of features vary according to the collecting and sampling methodologies applied to the network traffic. For instance, packets from NSL-KDD dataset have 42 features, while flows from CIDDs-001 dataset have 10. This information gap makes flow classification inherently less accurate than packet classification. Nevertheless, flow-based approaches are seen as good alternatives to precede packet inspection in real-time NIDSs. The idea is to deeply inspect only the packets belonging to flows considered to be suspicious by the flow-based classifier. A two-step approach would notably reduce the amount of data analyzed, while maintaining a high classification accuracy [2]. However, there are still some open questions in the field regarding how many and which features should be taken into account for classification. Trying to address these questions, in the next section we are going to characterize some features distribution within different flow classes.

B. Feature characterization

In order to perform a comprehensive feature characterization, a network trace containing different flow classes is necessary. The chosen flow dataset, CIDDs-001 [4], is a relatively recent dataset composed of a set of flow samples captured within a simulated OpenStack environment and another set of flow samples captured in an external server. The former contains only simulated traffic, while the latter contains both real and simulated traffic.

Each sample collected within the simulated environment has one of the labels described in the following:

- *normal* - normal traffic;
- *dos* - Denial of Service (DoS) attack traffic;
- *portScan* - port scan attack traffic;
- *pingScan* - ping scan attack traffic;
- *bruteForce* - brute force attack traffic.

Flows labeled as *dos*, *portScan*, *pingScan* or *bruteForce* are malicious flows. Each malicious flow is labeled regarding its origin as either *attacker* or *victim*. Flows sampled within the external server environment may have two extra labels, i.e., *suspicious* and *unknown*. Traffic was sampled in both the simulated and the external environment during a four week period. For the simulated environment, we consider only traffic captured in the second week to reduce the amount of data to be analyzed. Similarly, only external traffic captured within the third week was assessed. CIDDs-001 dataset flow features are shown in Table I. All features within Table I were taken into account for characterization and classification except for *Src IP*, *Dest IP* and *Date first seen*.

In order to evaluate the relationship between flow features and traffic classification, we characterized how normal/malicious traffic fractions change in response to constraining a given feature. To perform this analysis, 2,000 flows with each of the following labels: *normal*, *dos*, *portScan*, *pingScan*, and

Table I
FEATURES WITHIN CIDDs-001 DATASET

| # | Name | Description |
|----|-----------------|--|
| 1 | Src IP | Source IP Address |
| 2 | Src Port | Source Port |
| 3 | Dest IP | Destination IP Address |
| 4 | Dest Port | Destination Port |
| 5 | Proto | Transport Protocol (e.g., ICMP, TCP, or UDP) |
| 6 | Date first seen | Start time flow first seen |
| 7 | Duration | Duration of the flow |
| 8 | Bytes | Number of transmitted bytes |
| 9 | Packets | Number of transmitted packets |
| 10 | Flags | OR concatenation of all TCP Flags |

bruteForce were sampled from the simulated traffic within dataset CIDDs-001. Afterwards, the number of flows with a given feature value smaller than or equal to a given upper limit in each class was counted. Similarly, the same was done for decreasing upper limits of the same feature.

Figure 1 A) shows the normal/malicious traffic fractions for different upper limits considering the source port feature. It is possible to observe some anomalous patterns since malicious traffic fraction does not decrease in the same rate as normal traffic fraction. For instance, normal traffic fraction presents a near linear decrease. Since there is no TCP or UDP port number associated to ICMP protocol, ping scan traffic within CIDDs-001 dataset has source port value equal to 0. Given that, ping scan attack is perceived as coming mainly from a source "port" smaller than 50, and, consequently, its traffic fraction remains constant. For DoS, port scan and brute force attacks, their traffic fractions present an abrupt decrease between ports 50,000 and 10,000, showing that traffic of these types comes mostly from higher ports.

Normal/malicious traffic fractions for different upper limits of destination port are shown in Figure 1 B). It is possible to see that the anomalous patterns observed in B) change considerably in comparison to A), because malicious traffic comes from higher ports and is mainly aimed at smaller ports. While normal fraction decreases almost linearly, for DoS and brute force there is an abrupt decrease, since DoS traffic is mainly aimed at port 80 and brute force traffic at port 22. Here again it is important to notice that there is no TCP or UDP port number associated to ICMP protocol, so ping scan traffic within CIDDs-001 dataset has destination port value equal to 8. Destination port feature for port scan attack cannot be used to detect an anomalous behavior considering its nearly proportional fraction change.

Figure 1 C) shows the normal/malicious traffic fractions for different upper limits of feature number of bytes. Anomalous patterns can be observed considering the number of bytes for all attacks, since normal/malicious traffic fractions decrease at different rates. For instance, DoS traffic presents an abrupt decrease after 500, showing that all flows have 500 bytes or more. This is characteristic of volumetric DoS, which intends to flood the victim with traffic. Port/ping scan traffic fractions have slower decreases, since these types of flows tend to have number of bytes below 60. Meanwhile, like in previous cases,

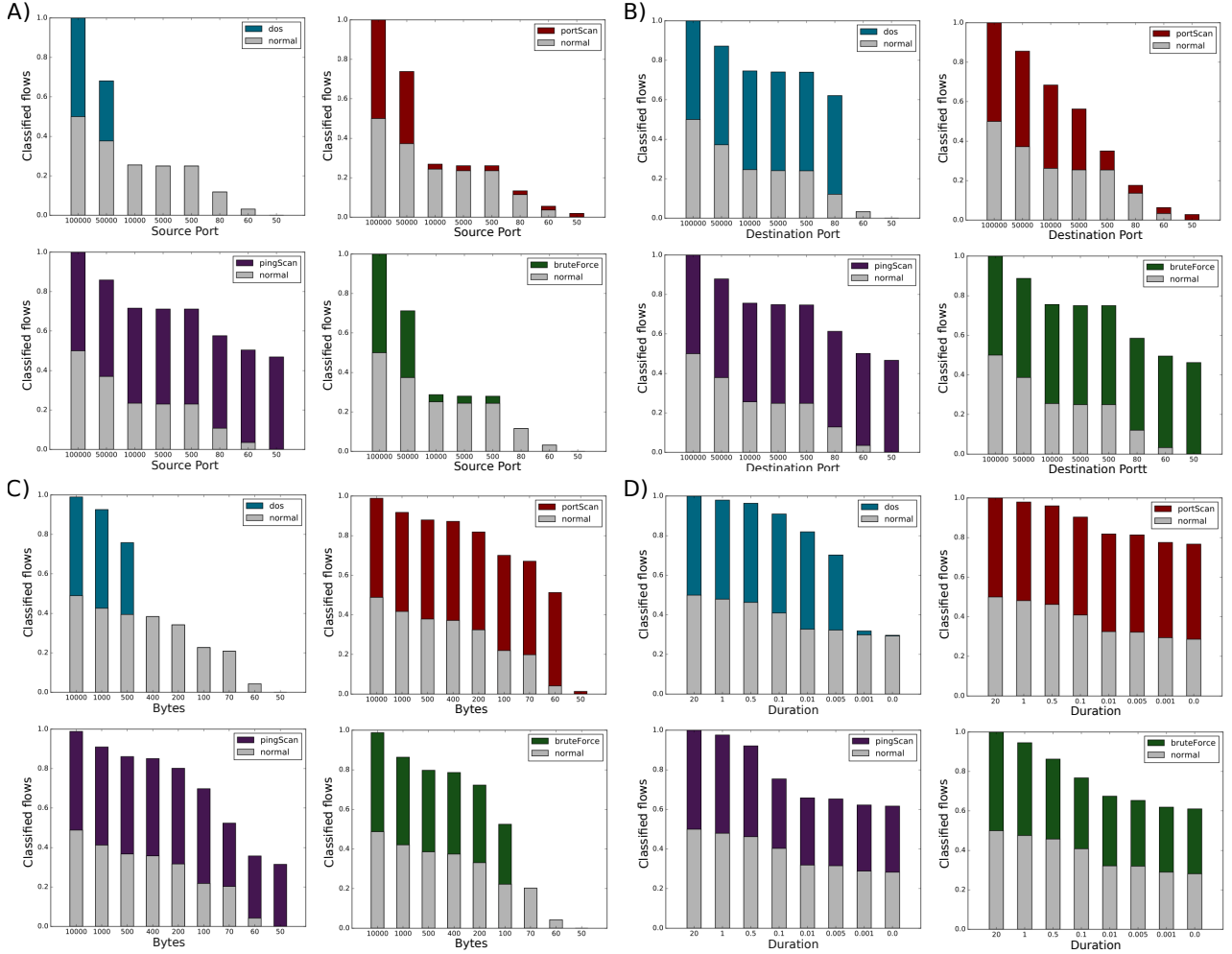


Figure 1. Normal/malicious traffic fractions for different upper limits of A) source port, B) destination port, C) number of bytes, and D) duration.

normal traffic fraction decreases almost linearly.

Finally, normal/malicious traffic fractions for different upper limits of duration are shown in Figure 1 D). Regarding feature duration, the normal/malicious traffic fractions decrease is proportional for most cases. The only exception is DoS traffic, which presents an abrupt decrease on 0.005 meaning that most flows belonging to this class have duration above 0.001.

Noticeably, the decremental change of the flow features enabled the detection of malicious traffic in a not very effective way. Our main contribution is to provide a mechanism able to combine the different features to perform sharper detection of malicious traffic considering abnormal behavior by combining multiple features. We construct a model based on flow features patterns present in normal traffic using inverse statistical physics to perform traffic classification, such as presented in the next section.

IV. STATISTICAL MODEL

The main task of inverse statistical physics is to infer a statistical distribution based on a sample of it [14]. Methods using inverse statistical physics have been successfully applied to problems in other disciplines, *e.g.*, the problem of predicting

protein contacts in Biophysics [14], [15]. Here, the statistical inference is based on the Potts model [16]. This model provides a mathematical description of interacting spins on a crystalline lattice. Within the model framework, interacting spins are mapped into a graph $G(\eta, \epsilon)$ (see Figure 2 A)), where each node $i \in \eta = \{1, \dots, N\}$ has an associated spin a_i , which can assume one value from a set Ω that contains all possible individual quantum states. Each node i has also an associated local field $h_i(a_i)$ that is a function of a_i 's state. Meanwhile, each edge $(i, j) \in \epsilon$, $i, j \in \eta$, has an associated coupling value $e_{ij}(a_i, a_j)$ that is a function of the states of spins a_i and a_j associated to nodes i and j . A specific system configuration has an associated total energy, determined by the Hamiltonian function $\mathcal{H}(a_1 \dots a_N)$, which depends on all spin states.

In this work, we adapt the Potts model to characterize network flows (see Figure 2 B)). An individual flow k is represented by a specific graph configuration $G_k(\eta, \epsilon)$. Instead of spins, each node represents a selected feature $i \in \eta = \{SrcPort, \dots, Flags\}$. Within a given flow k , each feature i assumes one value a_{ki} from the set Ω_i that contains all possible values for this feature. As in the Potts Model, each feature i has an associated local field $h_i(a_{ki})$. Meanwhile,

$\mathcal{E} = \{(i, j) | i, j \in \eta; i \neq j\}$ is the set of edges determined by all possible pairs of features. Each edge has an associated coupling value determined by the function $e_{ij}(a_{ki}, a_{kj})$.

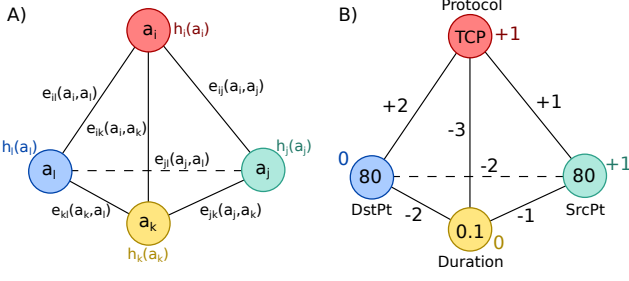


Figure 2. A) Interacting spins on a crystalline lattice. B) Network flow mapped into a graph structure.

Since the values of local fields and couplings depend on the values assumed by features within a given flow, each distinct flow will have a different combination of these quantities. As in the Potts Model, local fields and couplings determine the total "energy" $\mathcal{H}(a_{k1}...a_{kN})$ of each flow. For instance, in Figure 2 B), the total "energy" of the flow is obtained by summing up all values associated to the edges and to the nodes, resulting in a total of -3. Note that what we call energy is analogous to the notion of Hamiltonian in Quantum Mechanics.

It is important to note that the model described here is discrete, ergo continuous features must be discretized. The classes for continuous features discretization were defined based on the analysis performed in the last section and are shown on Appendix A. In the following, we present the framework applied to perform the statistical model inference and subsequent energy-based flow classification.

A. Model inference

In this section, coupling and local field values are going to be inferred from a statistical model to perform energy-based flow classification. The main idea consists in extracting a statistical model from benign flow samples to infer coupling and local field values that characterize this type of traffic. When calculating the energies of unlabeled flows using the inferred values, it is expected that benign flows will have lower energies than malicious flows.

Let $(A_1...A_N)$ be a N-uple of features, which can be instantiated for flow k as $(a_{k1}...a_{kN})$, with $a_{k1} \in \Omega_1, \dots, a_{kN} \in \Omega_N$. Each feature value a_{ki} is encoded by an integer from the set $\Omega = \{1, 2, \dots, Q\}$, i.e., all feature alphabets are the same $\Omega_i = \Omega$ of size Q . If a given feature can only assume M values and $M < Q$, it is considered that values $M+1, \dots, Q$ are possible, but will never be observed empirically. For instance, if the only possible values for feature *protocol* are $\{TCP, UDP\}$, and given $Q = 4$. In this case, we would have the mapping $\{TCP:1, UDP:2, ' ':3, ' ':4\}$ and feature values 3 and 4 would never occur.

Now, let \mathcal{K} be the set of all possible flows, i.e., all possible combinations of feature values ($\mathcal{K} = \Omega^N$), and let $\mathcal{S} \subset \mathcal{K}$ be a sample of flows. We can use inverse statistical

physics to infer a statistical model associating a probability $P(a_{k1}...a_{kN})$ to each flow $k \in \mathcal{K}$ based on sample \mathcal{S} . The global statistical model P is inferred following the Entropy Maximization Principle [17]:

$$\max_P - \sum_{k \in \mathcal{K}} P(a_{k1}...a_{kN}) \log(P(a_{k1}...a_{kN})) \quad (1)$$

s.t.

$$\sum_{k \in \mathcal{K} | a_{ki}=a_i} P(a_{k1}...a_{kN}) = f_i(a_i) \quad (2)$$

$$\forall i \in \eta; \forall a_i \in \Omega;$$

$$\sum_{k \in \mathcal{K} | a_{ki}=a_i, a_{kj}=a_j} P(a_{k1}...a_{kN}) = f_{ij}(a_i, a_j) \quad (3)$$

$$\forall (i, j) \in \eta^2 | i \neq j; \forall (a_i, a_j) \in \Omega^2;$$

where $f_i(a_i)$ is the empirical frequency of value a_i on feature i and $f_{ij}(a_i, a_j)$ is the empirical joint frequency of the pair of values (a_i, a_j) of features i and j . Note that constraints 2 and 3 force model P to generate single as well as joint empirical frequency counts as marginals. This way, the model is sure to be coherent with empirical data.

Single and joint empirical frequencies $f_i(a_i)$ and $f_{ij}(a_i, a_j)$ are obtained from set \mathcal{S} by counting occurrences of a given feature value a_i or feature value pair (a_i, a_j) , respectively, and dividing by the total number of flows in \mathcal{S} . Since the set \mathcal{S} is finite and much smaller than \mathcal{K} , inferences based on \mathcal{S} are subjected to undersampling effects. Following the theoretical framework proposed in [15], we add pseudocounts to empirical frequencies to limit undersampling effects by performing the following operations:

$$f_i(a_i) \leftarrow (1 - \alpha)f_i(a_i) + \frac{\alpha}{Q} \quad (4)$$

$$f_{ij}(a_i, a_j) \leftarrow (1 - \alpha)f_{ij}(a_i, a_j) + \frac{\alpha}{Q^2} \quad (5)$$

where $(a_i, a_j) \in \Omega^2$ and $0 \leq \alpha \leq 1$ is a parameter defining the weight of the pseudocounts. The introduction of pseudocounts is equivalent to assuming that \mathcal{S} is extended with a fraction of flows with uniformly sampled features.

The proposed maximization can be solved using a Lagrangian function such as presented in [17], yielding the following Boltzmann-like distribution:

$$P^*(a_{k1}...a_{kN}) = \frac{e^{-\mathcal{H}(a_{k1}...a_{kN})}}{Z} \quad (6)$$

where

$$\mathcal{H}(a_{k1}...a_{kN}) = - \sum_{i,j | i < j} e_{ij}(a_{ki}, a_{kj}) - \sum_i h_i(a_{ki}) \quad (7)$$

is the Hamiltonian of flow k . In eq. (6), Z is the partition function that normalizes the distribution. Since in this work we are not interested in obtaining individual flow probabilities, Z is not required and, as a consequence, its calculation is omitted. Our objective is to calculate individual flows energies, i.e., individual Hamiltonians as determined in eq. (7).

Note that the Hamiltonian, as presented above, is fully determined in terms of the Lagrange multipliers $e_{ij}(\cdot)$ and

$h_i(\cdot)$ associated to constraints (2) and (3), respectively. Within the Potts Model framework, the Lagrange multipliers have a special meaning, with the set $\{e_{ij}(a_i, a_j) | (a_i, a_j) \in \Omega^2\}$ being the set of all possible coupling values between features i and j and $\{h_i(a_i) | a_i \in \Omega\}$ the set of possible local fields associated to feature i .

Inferring the local fields and pairwise couplings is difficult since the number of parameters exceeds the number of independent constraints. Due to the physical properties of interacting spins, it is possible to infer pairwise coupling values $e_{ij}(a_i, a_j)$ using a Gaussian approximation. Assuming that the same properties apply for flow features, we infer coupling values as follows:

$$e_{ij}(a_i, a_j) = -(C^{-1})_{ij}(a_i, a_j), \quad (8)$$

$$\forall (i, j) \in \eta^2, \forall (a_i, a_j) \in \Omega^2, a_i, a_j \neq Q$$

where

$$C_{ij}(a_i, a_j) = f_{ij}(a_i, a_j) - f_i(a_i)f_j(a_j) \quad (9)$$

is the covariance matrix obtained from single and joint empirical frequencies. Taking the inverse of the covariance matrix is a well known procedure in statistics to remove the effect of indirect correlation in data [18]. Here, it is important to clarify that, the number of independent constraints in eq. (2) and eq. (3) is actually $\frac{N(N-1)}{2}(Q-1)^2 + N(Q-1)$, even though the model in eq. (6) has $\frac{N(N-1)}{2}Q^2 + NQ$ parameters. So, without loss of generality, we set:

$$e_{i,j}(a_i, Q) = e_{i,j}(Q, a_j) = h_i(Q) = 0 \quad (10)$$

Thus, in eq. (8) there is no need to calculate $e_{i,j}(a_i, a_j)$ in case a_i or a_j is equal to Q [15]. Afterwards, local fields $h_i(a_i)$ can be inferred using a mean-field approximation [19]:

$$\frac{f_i(a_i)}{f_i(Q)} = \exp \left(h_i(a_i) + \sum_{j,a_j} e_{ij}(a_i, a_j) f_j(a_j) \right), \quad (11)$$

$$\forall i \in \eta, a_i \in \Omega, a_i \neq Q$$

where $f_i(Q)$ is the frequency of the last element $a_i = Q$ for any feature i used for normalization. It is also worth mentioning that the element Q is arbitrarily selected and could be replaced by any other value in $\{1 \dots Q\}$ as long as the selected element is kept the same for calculations of the local fields of every feature $i \in \eta$. Note that in eq. (11) the empirical single frequencies $f_i(a_i)$ and the coupling values $e_{ij}(a_i, a_j)$ are known, yielding:

$$h_i(a_i) = \ln \left(\frac{f_i(a_i)}{f_i(Q)} \right) - \sum_{j,a_j} e_{ij}(a_i, a_j) f_j(a_j) \quad (12)$$

In the mean-field approximation presented above, the interaction of a feature with its neighbors is replaced by an approximate interaction with an averaged feature, yielding an approximated value for the local field associated to it.

For further details about this calculations please refer to [14]. Now that all model parameters are known, it is possible to calculate a given flow energy according to eq. (7). In the following, we are going to present the theoretical framework implementation to perform a two-class, *i.e.*, normal and malicious, flow classification.

B. Energy-based flow classification

The energy of a given flow can be calculated according to eq. (7) based on the values of its features and the parameters from the statistical model inferred in the last section. In simple terms, a given flow energy is the negative sum of couplings and local fields associated to its features, according to a given statistical model. It means that, if a flow resembles the ones used to infer the model, it is likely to be low in energy. This happens because features that were strongly coupled in sample \mathcal{S} that generated the model, are going to be present in that flow.

Since EFC is an anomaly-based classifier, the statistical model used for classification is inferred based on normal flow samples. We would then expect energies of normal samples to be lower than energies of malicious samples. In this sense, it is possible to classify flow samples as normal or malicious based on a chosen energy threshold. The classification is performed by stating that samples with energy smaller than the threshold are normal and samples with energy greater than or equal to the threshold are malicious. Note that the threshold for classification can be chosen in different ways and it can be static or dynamic. In this work we will consider a static threshold.

Algorithm 1 implements the first step for model inference, considering equation (4) to calculate empirical single frequencies. On lines 3-7 the frequencies of each feature value in each column are counted. On line 8, frequency values are reweighted using pseudocount parameter α . In the end, this function produces a two-dimensional array with shape (N, Q) , where N is the number of features considered and Q is the cardinality of the alphabet. This array contains the empirical frequencies of each possible value for all features.

Algorithm 1 One-site empirical frequencies

```

1: function SITEFREQ( $flows_{(K \times N)}$ ,  $Q$ ,  $\alpha$ )
2:   matrix  $f\_i_{(N \times Q)}$ 
3:   for  $i \leftarrow 1$  to  $N$  do
4:     for  $a\_i \leftarrow 1$  to  $Q$  do
5:        $f\_i[i, a\_i] \leftarrow \text{count}(a\_i, flows[:, i]) / K$ 
6:     end for
7:   end for
8:    $f\_i \leftarrow (1 - \alpha)f\_i + \alpha/Q$ 
9:   return  $f\_i$ 
10: end function

```

Joint frequencies from equation (5), in turn, are calculated as described in Algorithm 2. On lines 3-8, the occurrences of each possible feature value pair are counted. Afterwards, on line 9, pairwise frequency values are reweighted using pseudocount parameter α . On lines 10-18, to correct inconsistencies caused by the pseudocounts, elements in the diagonal are set to 0.0 in case $a_i \neq a_j$ and to $f_i(a_i)$ otherwise, since there is no meaning in pairing one feature with itself. The output of this function is an array with shape (N, Q, N, Q) containing the joint empirical frequencies of each possible pair of values (Q^2 possibilities) for each pair of features (N^2 possibilities).

After single and joint empirical frequencies are computed according to equation (8), coupling values are obtained as

Algorithm 2 Two-site empirical frequencies

```

1: function PAIRFREQ( $flows_{(K \times N)}$ ,  $f\_i_{(N \times Q)}$ ,  $Q$ ,  $\alpha$ )
2:   matrix  $f\_ij_{(N \times Q \times N \times Q)}$ 
3:   for  $(i, j) \leftarrow [(1, 1), (1, 2), \dots, (N, N)]$  do
4:     for  $(a\_i, a\_j) \leftarrow [(1, 1), (1, 2), \dots, (Q, Q)]$  do
5:        $is\_pair \leftarrow [1 \text{ for } k \text{ in } [1..K] \text{ if } (flows[k, i] = a\_i$ 
         and  $flows[k, j] = a\_j)]$ 
6:        $f\_ij[i, a\_i, j, a\_j] \leftarrow count(1, is\_pair)/K$ 
7:     end for
8:   end for
9:    $f\_ij \leftarrow (1 - \alpha)f\_ij + \alpha/Q^2$ 
10:  for  $i \leftarrow 1$  to  $N$  do
11:    for  $(a\_i, a\_j) \leftarrow [(1, 1), (1, 2), \dots, (Q, Q)]$  do
12:      if  $a\_i = a\_j$  then
13:         $f\_ij[i, a\_i, i, a\_j] \leftarrow f\_i[i, a\_i]$ 
14:      else
15:         $f\_ij[i, a\_i, i, a\_j] \leftarrow 0.0$ 
16:      end if
17:    end for
18:  end for
19:  return  $f\_ij$ 
20: end function

```

Algorithm 3 Coupling values inference

```

1: function COUPLINGS( $f\_i_{(N \times Q)}$ ,  $f\_ij_{(N \times Q \times N \times Q)}$ ,  $Q$ )
2:   matrix  $cov_{(N \times Q - 1 \times N \times Q - 1)}$ 
3:   for  $(i, j) \leftarrow [(1, 1), (1, 2), \dots, (N, N)]$  do
4:     for  $(a\_i, a\_j) \leftarrow [(1, 1), (1, 2), \dots, (Q - 1, Q - 1)]$  do
5:        $cov[i, a\_i, j, a\_j] \leftarrow f\_ij[i, a\_i, j, a\_j] -$ 
          $f\_i[i, a\_i]f\_i[j, a\_j]$ 
6:     end for
7:   end for
8:    $e\_ij \leftarrow -cov^{-1}$ 
9:   return  $e\_ij$ 
10: end function

```

described in Algorithm 3. On lines 3-7, the covariance matrix is build, and on line 8 the negative of its inverse is computed. In the end, this functions returns an array with shape $(N \times (Q - 1), N \times (Q - 1))$ containing the negative inverse of the covariance matrix, *i.e.*, the values of couplings $e_{ij}(a_i, a_j), \forall (i, j) \in \eta^2, (a_i, a_j) \in \Omega^2$.

Afterwards, local fields from equation (12) are computed as described in Algorithm 4. On line 5, local field $h_i(a_i)$ is initialized as $\ln\left(\frac{f_i(a_i)}{f_i(Q)}\right)$. After that $h_i(a_i)$ is decremented by the values of the couplings $e_{ij}(a_i, a_j)f_j(a_j)$ for all possible values of j and a_j . The output of this function is an array with shape $(N, Q - 1)$, containing the values of the local fields $h_i(a_i), \forall i \in \eta, a_i \in \Omega$.

Finally, Algorithm 5 shows the implementation of EFC. On lines 2-5, the statistical model for the sampled flows is inferred using the functions described in Algorithms 1-4. Afterwards, on lines 6-27, the classifier monitors the network waiting for a captured flow. When a flow is captured, its energy is calculated on lines 9-20, according to the Hamiltonian involving the received flow features in equation (7). The computed flow energy is compared to a known threshold (*cutoff*) value on

Algorithm 4 Local fields inference

```

1: function LOCALFIELDS( $e\_ij_{(N \times Q - 1 \times N \times Q - 1)}$ ,
   $f\_i_{(N \times Q)}$ ,  $Q$ )
2:   matrix  $h\_i_{(N \times Q - 1)}$ 
3:   for  $i \leftarrow 1$  to  $N$  do
4:     for  $a\_i \leftarrow 1$  to  $Q - 1$  do
5:        $h\_i[i, a\_i] \leftarrow \ln(f\_i[i, a\_i]/f\_i[i, Q])$ 
6:       for  $j \leftarrow 1$  to  $N$  do
7:         for  $a\_j \leftarrow 1$  to  $Q - 1$  do
8:            $h\_i[i, a\_i] \leftarrow h\_i[i, a\_i] -$ 
              $e\_ij[i, a\_i, j, a\_j]f\_i[j, a\_j]$ 
9:         end for
10:       end for
11:     end for
12:   end for
13:   return  $h\_i$ 
14: end function

```

Algorithm 5 Energy-based Flow Classifier

Input: $normal_flows_{(K \times N)}$, Q , α , *cutoff*

```

1: import all model inference functions
2:  $f\_i \leftarrow SiteFreq(normal\_flows, Q, \alpha)$ 
3:  $f\_ij \leftarrow PairFreq(normal\_flows, f\_i, Q, \alpha)$ 
4:  $e\_ij \leftarrow Couplings(f\_i, f\_ij, Q)$ 
5:  $h\_i \leftarrow LocalFields(e\_ij, f\_i, Q)$ 
6: while Scanning the Network do
7:    $flow \leftarrow wait\_for\_incoming\_flow()$ 
8:    $e \leftarrow 0$ 
9:   for  $i \leftarrow 1$  to  $N - 1$  do
10:     $a\_i \leftarrow flow[i]$ 
11:    for  $j \leftarrow i + 1$  to  $N$  do
12:       $a\_j \leftarrow flow[j]$ 
13:      if  $a\_i \neq Q$  and  $a\_j \neq Q$  then
14:         $e \leftarrow e - e\_ij[i, a\_i, j, a\_j]$ 
15:      end if
16:    end for
17:    if  $a\_i \neq Q$  then
18:       $e \leftarrow e - h\_i[i, a\_i]$ 
19:    end if
20:  end for
21:  if  $e < cutoff$  then
22:    stop_flow()
23:    forward_to_DPI()
24:  else
25:    release_flow()
26:  end if
27: end while

```

line 21. In case the energy falls bellow the threshold, the flow is classified as malicious and should be forwarded to deep packet inspection (line 23) for assessment. Otherwise, the flow is released and the classifier waits for another flow. Considering this implementation, next, we present the results obtained when EFC is used to perform flow classification.

V. RESULTS

In this section, we describe and discuss the results obtained regarding the statistical model properties and the classification tests performed on dataset CIDDs-001. First, we show that the statistical model recovers important traffic properties from the flow set used in the model building phase. Then it is shown that the statistical model built based on normal traffic samples is able to separate normal from malicious flows based on their energies. Finally, we present the classification results obtained for EFC and compare them to results obtained for other classifiers in two different test scenarios.

A. Model analysis

Tables II - VI show the most strongly coupled variables in the statistical models inferred based on traffic labeled as *normal*, *dos*, *portScan*, *pingScan* and *bruteForce*, respectively. Entries present in Tables III - VI but not in Table II are in bold. By looking at the top 5 couplings in different statistical models, it is possible to see that each model is characterized by different coupling patterns.

Table II
TOP 5 COUPLING VALUES OBTAINED FROM STATISTICAL MODEL
INFERRED BASED ON FLOWS LABELED AS NORMAL

| Feature i | Value a_i | Feature j | Value a_j | $e_{ij}(a_i, a_j)$ |
|-------------|-------------|-------------|-------------|--------------------|
| Protocol | UDP | Flags | | 19.5 |
| Src Pt | 100-400 | Dst Pt | 100-400 | 12.6 |
| Duration | 0.000 | Packets | 1 | 11.8 |
| Protocol | TCP | ToS | 32 | 11.4 |
| Bytes | 60-70 | Flags | .A.... | 11.0 |

Table III
TOP 5 COUPLING VALUES OBTAINED FROM STATISTICAL MODEL
INFERRED BASED ON FLOWS LABELED AS DOS

| Feature i | Value a_i | Feature j | Value a_j | $e_{ij}(a_i, a_j)$ |
|----------------|-------------|--------------|----------------|--------------------|
| Protocol | UDP | Flags | | 17.9 |
| Packets | 5 | Bytes | 400-500 | 15.3 |
| Packets | 6 | Bytes | 500-700 | 14.5 |
| Duration | 0.000 | Packets | 1 | 13.4 |
| Bytes | 60-70 | Flags | .A.... | 12.0 |

Table IV
TOP 5 COUPLING VALUES OBTAINED FROM STATISTICAL MODEL
INFERRED BASED ON FLOWS LABELED AS PORT SCAN

| Feature i | Value a_i | Feature j | Value a_j | $e_{ij}(a_i, a_j)$ |
|-----------------|--------------|---------------|---------------|--------------------|
| Protocol | UDP | Flags | | 15.8 |
| Duration | 0.000 | Packets | 1 | 14.3 |
| Bytes | 50-60 | Flags |S. | 12.9 |
| Protocol | ICMP | Src Pt | 0-50 | 11.8 |
| Src Pt | 0-50 | Bytes | 0-50 | 11.6 |

It is important to note that feature anomalies which characterize different classes of malicious flows in figure 1 are strongly coupled in the respective statistical models presented in this section. These results reinforce the conclusion that malicious flows present, in fact, statistically meaningful anomalies in their features. Moreover, Tables II - VI show that the statistical approach proposed here is capable to capture these anomalies.

Table V
TOP 5 COUPLING VALUES OBTAINED FROM STATISTICAL MODEL
INFERRED BASED ON FLOWS LABELED AS PING SCAN

| Feature i | Value a_i | Feature j | Value a_j | $e_{ij}(a_i, a_j)$ |
|-----------------|-------------|---------------|-------------|--------------------|
| Duration | 0.000 | Packets | 1 | 14.7 |
| Protocol | UDP | Flags | | 14.6 |
| Protocol | ICMP | Src Pt | 0-50 | 14.3 |
| Protocol | ICMP | Dst Pt | 0-50 | 14.0 |
| Src Pt | 0-50 | Dst Pt | 0-50 | 14.0 |

Table VI
TOP 5 COUPLING VALUES OBTAINED FROM STATISTICAL MODEL
INFERRED BASED ON FLOWS LABELED AS BRUTE FORCE

| Feature i | Value a_i | Feature j | Value a_j | $e_{ij}(a_i, a_j)$ |
|---------------|-------------|--------------|---------------|--------------------|
| Protocol | UDP | Flags | | 18.7 |
| Src Pt | 100-400 | Dst Pt | 100-400 | 16.7 |
| Duration | 0.000 | Packets | 1 | 14.0 |
| Bytes | 60-70 | Flags | .A.... | 12.8 |
| Dst Pt | 0-50 | Flags |S. | 12.7 |

In Figure 3, flow energies calculated using a statistical model based on normal traffic are shown. The histogram shows energy values of 5,000 randomly sampled flows labeled as *normal* and 5,000 randomly sampled flows labeled as *malicious* from the simulated traffic contained in CIDDs-001. The statistical model used to calculate the energies was inferred based on 4,500 flows randomly sampled from the simulated traffic dataset. The separation between the two flow classes considered, *i.e.*, normal and malicious, is clear. Normal flow energy distribution is clearly shifted to the left in relation to malicious flow energy distribution. A chosen energy threshold value used to separate classes is shown in red.

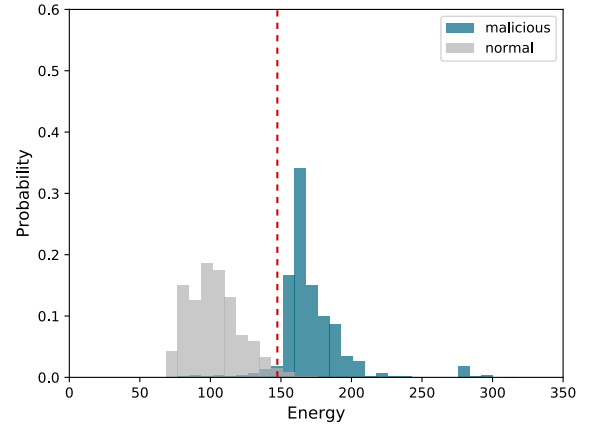


Figure 3. Energy histogram for flow samples in test set I (simulated).

Figure 4 shows flow energies calculated based on the same statistical model, however, coming from the external server traffic scenario. The histogram shows energy values of 5,000 randomly sampled flows labeled as *unknown* and 5,000 randomly sampled flows labeled as *suspicious* from the external server traffic in CIDDs-001. Traffic labeled as *unknown* is traffic coming from external users with destination port 80 or 443, *i.e.*, expected traffic. In this sense, here we consider

this traffic to be analogous to normal traffic. Traffic labeled as *suspicious*, on the other hand, is traffic coming from external users aimed at ports other than 80 and 443, *i.e.*, unexpected traffic. Hence, this traffic is considered here analogous to malicious traffic. Note that the separation between this two classes, *i.e.*, unknown and suspicious, is also clear. In Figure 4 we can see that a portion of unknown traffic is mixed up with suspicious traffic, which might be an indication that this traffic, even with expected destination ports, is actually malicious.

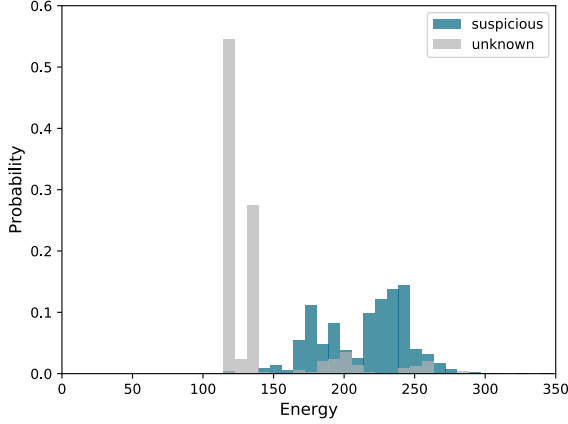


Figure 4. Energy histogram for flow samples in test set II (external).

It is important to note that we can apply the same energy threshold (around 150) to separate the two classes in both the simulated and the external traffic contexts. Because the threshold learned in the simulated traffic scenario can be applied to separate the traffic in the external server scenario, we understand that the statistical model learned is resilient to context change. In the following section, classification results are shown for different classifiers and compared with the results obtained with EFC.

B. Classification results

In this subsection we describe how the test sets were constructed and how the training and testing processes were performed. Next, we present the classification results obtained for EFC and compare them to results obtained for other classifiers.

To evaluate the performance of different ML algorithms and EFC, we constructed test sets using a subset of CIDDs-001 dataset, as described in the following. The first 100,000 non-redundant flows labeled as *normal* were extracted from week 2 simulated traffic to compose a normal traffic sampling pool. Week 2 was chosen because attacks from different types are more equally distributed on this week than on the other weeks. Similarly, a malicious traffic sampling pool was composed. All flows labeled as *pingScan* and *bruteForce* were extracted from within week 2 simulated traffic. In addition, the first 90,000 non-redundant DoS flows and the first 9,000 non-redundant port scan flows were selected to compose this pool. Dataset undersampling was performed in order to obtain a more homogeneous distribution of the different malicious

traffic subclasses. Also, because we want to focus on incoming traffic classification, malicious traffic labeled as *victim* was not selected to compose the sampling pool. Afterwards, 5,000 normal flows and 5,000 malicious flows were sampled from the normal traffic pool and the malicious traffic pool, respectively to compose a set of size 10,000 which was validated using a 10-fold cross validation (see Appendix B). Since flows labeled as *pingScan* and *bruteForce* were rare, all samples with these labels were included in the test set.

Similarly, the first non-redundant 16,900 unknown flows and the first non-redundant 47,700 suspicious flows were extracted from CIDDs-001 week 3 external server traffic. Week 3 was chosen because suspicious and unknown flows are more equally distributed on this week than on the other weeks. A set with 5,000 suspicious and 5,000 unknown flows randomly sampled from the suspicious traffic pool and the unknown traffic pool, respectively, was constructed and validated using a 10-fold cross validation (see Appendix B). Data within the test set was only discretized for EFC, since discretization would probably impair the performance of most ML algorithms.

To assess the performance of EFC, we deployed eight ML classifiers found in [20] that are available online at GitHub¹. The deployed classifiers are: KNN, Decision Tree (DT), Adaboost, Random Forest (RF), Artificial Neural Network (ANN), Linear Regression (LR), Naive Bayes (NB), and polynomial SVM. All classifiers were deployed with their default scikit-learn configurations. Table VII shows classification results for all test sets considering that all classifiers as well as EFC were trained with the same training set. The only difference regarding the training of the classifiers is that EFC is only trained with normal traffic. The metric used to compare the results is the accuracy, calculated as follows:

$$Acc = \frac{TPR + TNR}{2} \quad (13)$$

where TPR is the true positive rate, *i.e.*, percentage of normal traffic classified as normal, and TNR stands for true negative rate, *i.e.*, percentage of malicious traffic classified as malicious.

Table VII
CLASSIFICATION RESULTS - DIFFERENT CLASSIFIERS TRAINED WITH SIMULATED TRAFFIC

| Classifier | Test set I (simulated) | | | Test set II (external) | | |
|------------|------------------------|-------|----------------------|------------------------|-------|----------------------|
| | TNR | TPR | Acc | TNR | TPR | Acc |
| LR | 0.971 | 0.500 | 0.736 ± 0.013 | 0.502 | 0.416 | 0.459 ± 0.009 |
| Gauss. NB | 0.170 | 0.957 | 0.564 ± 0.042 | 0.748 | 0.338 | 0.543 ± 0.011 |
| KNN | 0.979 | 0.985 | 0.982 ± 0.005 | 0.180 | 0.694 | 0.437 ± 0.007 |
| DT | 0.984 | 0.996 | 0.990 ± 0.005 | 0.384 | 0.436 | 0.410 ± 0.017 |
| Adaboost | 0.983 | 0.989 | 0.986 ± 0.006 | 0.360 | 0.915 | 0.638 ± 0.009 |
| RF | 0.988 | 0.996 | 0.992 ± 0.005 | 0.260 | 0.975 | 0.618 ± 0.015 |
| Poly. SVM | 0.992 | 0.501 | 0.746 ± 0.006 | 0.505 | 0.397 | 0.451 ± 0.010 |
| ANN | 0.944 | 0.986 | 0.965 ± 0.006 | 0.501 | 0.905 | 0.703 ± 0.009 |
| EFC | 0.948 | 0.984 | 0.966 ± 0.007 | 0.980 | 0.847 | 0.913 ± 0.004 |

It is clear from Table VII that most classifiers achieve high accuracy processing test set I (simulated traffic). For instance, KNN, DT, Adaboost and RF achieved over 0.980 accuracy. ANN did also obtain good results (Acc = 0.965). LR, NB and

¹<https://github.com/vinayakumarr/Network-Intrusion-Detection>

polynomial SVM, on the other hand, did not obtain very good results. On test set II (external traffic), only EFC achieves accuracy over 0.900, showing that EFC is resilient to context change regarding both the simulated and external environments from dataset CIDDs-001. Such context resilience is a highly desirable trait in a flow-based classifier, since NIDSs classifiers are trained usually in a synthetic environment to be later applied in real context. Moreover, EFC is the only considered classifier that is independent of malicious flow samples to be trained and could easily learn from real data instead, achieving almost the same performance. In the following, we present our conclusions and future work.

VI. CONCLUSION

The results presented in the last section show three important and distinguishing characteristics of EFC. First, EFC is capable of separating benign from malicious flows based on energy values using a model learned from benign traffic alone. Second, EFC was shown to be resilient to context change within dataset CIDDs-001, while all other classifiers were not. And third, EFC is easy to implement and does not perform costly operation, as shown in Section IV-B.

Considering the advantages presented, we believe EFC to be a promising algorithm to perform flow-based traffic classification. Nevertheless, despite the promising results achieved, there is still room for further testing and improvement. For instance, in order to obtain a more homogeneous distribution of different attack types, we performed a dataset undersampling, which might have had some effect on the results. Hence, in future work we aim at performing a more comprehensive investigation of EFC applicability using different datasets (e.g., CICIDS [21]) and traffic captured in real networks to thoroughly test it.

APPENDIX A

Table VIII shows the classes used for feature discretization. Within CIDDs-001 dataset, TCP Flags is the discrete feature with more possible values (32 possibilities), so the alphabet size Q was set to 32. Each continuous feature values were clustered in a certain number of classes (or bins), up to Q classes. Classes were determined in such a way that the number of values within each class was similar for all classes.

Table VIII
CLASSES USED FOR FEATURE DISCRETIZATION

| Feature | List of classes upper limits |
|-----------------|--|
| Duration | 0.001, 0.002, 0.003, 0.004, 0.005, 0.006, 0.01, 0.04, 1, 10, 100, ∞ |
| Protocol | TCP, UDP, GRE, ICMP, IGMP |
| Src Port | 50, 60, 100, 400, 500, 40000, 60000, ∞ |
| Dst Port | 50, 60, 100, 400, 500, 40000, 60000, ∞ |
| Num. of Bytes | 50, 60, 70, 90, 100, 110, 200, 300, 400, 500, 700, 1000, 5000, ∞ |
| Num. of Packets | 2, 3, 4, 5, 6, 7, 10, 20, ∞ |
| TCP Flags | $\{(f_1, f_2, f_3, f_4, f_5) f_i \in \{0, 1\}\}$ |

APPENDIX B

Table IX shows the composition of two non-redundant sampling pools, which are a subset of CIDDs-001 dataset

used to construct the even smaller sets considered to evaluate classification accuracy. The composition of the sets used to assess classification performance is shown in Table X. These sets were validated using a 10-fold cross validation. Dataset undersampling was performed in order to obtain a more homogeneous distribution of the different classes of malicious traffic.

Table IX
STRUCTURE OF SAMPLING POOL FROM CIDDs-001 USED TO COMPOSE 10-FOLD CROSS VALIDATION SETS

| Class | Simulated (week 2) | External (week 3) |
|-------------------|--------------------|-------------------|
| <i>normal</i> | 100,000 | 0 |
| <i>attack</i> | 100,000 | 0 |
| <i>unknown</i> | 0 | 16,900 |
| <i>suspicious</i> | 0 | 47,700 |

Table X
FLOWS LABELS WITHIN 10-FOLD CROSS VALIDATION SETS

| Label | Simulated (week2) | External (week 3) |
|-------------------|-------------------|-------------------|
| <i>normal</i> | 5,000 | 0 |
| <i>dos</i> | 1,919 | 0 |
| <i>portScan</i> | 1,919 | 0 |
| <i>pingScan</i> | 152 | 0 |
| <i>bruteForce</i> | 910 | 0 |
| <i>suspicious</i> | 0 | 5,000 |
| <i>unknown</i> | 0 | 5,000 |
| <i>all</i> | 10,000 | 10,000 |

ACKNOWLEDGMENT

The authors would like to thank Luís Paulo Faina Garcia for helping with dataset analysis. Matt Bishop was supported by the National Science Foundation under Grant Number OAC-1739025. Any opinions, findings, and conclusions or recommendations expressed in this material are those of the author(s) and do not necessarily reflect the views of the National Science Foundation. João Gondim gratefully acknowledges the support from Project "EAGER: USBRCCR: Collaborative: Securing Networks in the Programmable Data Plane Era" funded by NSF and RNP (Brazilian National Research Network).

REFERENCES

- [1] Symantec, "Internet Security Threat Report (ISTR) 2019 | Symantec," Apr. 2019. [Online]. Available: <https://www.symantec.com/security-center/threat-report>
- [2] A. Sperotto, G. Schaffrath, R. Sadre, C. Morariu, A. Pras, and B. Stiller, "An overview of IP flow-based intrusion detection," *IEEE Communications Surveys and Tutorials*, vol. 12, no. 3, pp. 343–356, 2010. [Online]. Available: <http://ieeexplore.ieee.org/document/5455789/>
- [3] M. F. Umer, M. Sher, and Y. Bi, "Flow-based intrusion detection: Techniques and challenges," *Computers and Security*, vol. 70, pp. 238–254, sep 2017. [Online]. Available: <https://linkinghub.elsevier.com/retrieve/pii/S0167404817301165>
- [4] M. Ring, S. Wunderlich, D. Grödl, D. Landes, and A. Hotho, "Flow-based benchmark data sets for intrusion detection," in *Proceedings of the 16th European Conference on Cyber Warfare and Security. ACPI*, 2017, pp. 361–369.

- [5] P. Winter, E. Hermann, and M. Zeilinger, "Inductive intrusion detection in flow-based network data using one-class support vector machines," in *2011 4th IFIP international conference on new technologies, mobility and security*. IEEE, 2011, pp. 1–5.
- [6] N. Moustafa, B. Turnbull, and K.-K. R. Choo, "An ensemble intrusion detection technique based on proposed statistical flow features for protecting network traffic of internet of things," *IEEE Internet of Things Journal*, 2018.
- [7] B. A. Tama and K.-H. Rhee, "Attack classification analysis of iot network via deep learning approach," *Research Briefs on Information & Communication Technology Evolution (ReBICTE)*, vol. 3, pp. 1–9, 2017.
- [8] M. Idhammad, K. Afdel, and M. Belouch, "Distributed intrusion detection system for cloud environments based on data mining techniques," *Procedia Computer Science*, vol. 127, pp. 35–41, 2018.
- [9] —, "Detection system of http ddos attacks in a cloud environment based on information theoretic entropy and random forest," *Security and Communication Networks*, vol. 2018, 2018.
- [10] A. Verma and V. Ranga, "Statistical analysis of cids-001 dataset for network intrusion detection systems using distance-based machine learning," *Procedia Computer Science*, vol. 125, pp. 709–716, 2018.
- [11] M. Ring, D. Landes, and A. Hotho, "Detection of slow port scans in flow-based network traffic," *PloS one*, vol. 13, no. 9, p. e0204507, 2018.
- [12] R. Abdulhammed, M. Faezipour, A. Abuzneid, and A. AbuMallouh, "Deep and Machine Learning Approaches for Anomaly-Based Intrusion Detection of Imbalanced Network Traffic," *IEEE Sensors Letters*, vol. 3, no. 1, pp. 1–4, jan 2019. [Online]. Available: <https://ieeexplore.ieee.org/document/8526292/>
- [13] D. Plonka, "Flowsan: A network traffic flow reporting and visualization tool," in *LISA*, 2000, pp. 305–317.
- [14] S. Cocco, C. Feinauer, M. Figliuzzi, R. Monasson, and M. Weigt, "Inverse statistical physics of protein sequences: A key issues review," *Reports on Progress in Physics*, vol. 81, no. 3, p. 032601, mar 2018. [Online]. Available: <http://stacks.iop.org/0034-4885/81/i=3/a=032601?key=crossref.353cf55f4345afafde1886d057be92bd>
- [15] F. Morcos, A. Pagnani, B. Lunt, A. Bertolino, D. S. Marks, C. Sander, R. Zecchina, J. N. Onuchic, T. Hwa, and M. Weigt, "Direct-coupling analysis of residue coevolution captures native contacts across many protein families," *Proceedings of the National Academy of Sciences of the United States of America*, vol. 108, no. 49, pp. E1293–E1301, dec 2011. [Online]. Available: <http://www.pnas.org/cgi/doi/10.1073/pnas.1111471108>
- [16] F. Y. Wu, "The Potts model," *Reviews of Modern Physics*, vol. 54, no. 1, pp. 235–268, jan 1982. [Online]. Available: <https://link.aps.org/doi/10.1103/RevModPhys.54.235>
- [17] E. T. Jaynes, "Information theory and statistical mechanics. II," *Physical Review*, vol. 108, no. 2, pp. 171–190, may 1957. [Online]. Available: <https://link.aps.org/doi/10.1103/PhysRev.106.620>
- [18] B. Giraud, J. M. Heumann, and A. S. Lapedes, "Superadditive correlation," *Physical Review E*, vol. 59, no. 5, p. 4983, 1999.
- [19] A. Georges and J. S. Yedidia, "How to expand around mean-field theory using high-temperature expansions," *Journal of Physics A: Mathematical and General*, vol. 24, no. 9, p. 2173, 1991.
- [20] R. Vinayakumar, K. Soman, and P. Poornachandran, "Evaluating effectiveness of shallow and deep networks to intrusion detection system," in *2017 International Conference on Advances in Computing, Communications and Informatics (ICACCI)*. IEEE, 2017, pp. 1282–1289.
- [21] I. Sharafaldin, A. H. Lashkari, and A. A. Ghorbani, "Toward generating a new intrusion detection dataset and intrusion traffic characterization," in *ICISSP*, 2018, pp. 108–116.



Camila F. T. Pontes is a student at University of Brasilia (UnB), Brasilia, DF, Brazil. She received her M.Sc. degree in Molecular Biology in 2016 from UnB and is currently an undergrad student at the Department of Computer Science (CIC/UnB). Her research interests are Computational and Theoretical Biology, and Network Security.



João J. C. Gondim was awarded an M.Sc. in Computing Science at Imperial College, University of London, in 1987 and a Ph.D. in Electrical Engineering at UnB (University of Brasilia, 2017). He is an adjunct professor at Department of Computing Science (CIC) at UnB where he is a tenured member of faculty. His research interests are network, information and cyber security.



Matt Bishop received his Ph.D. in computer science from Purdue University, where he specialized in computer security, in 1984. His main research area is the analysis of vulnerabilities in computer systems. The second edition of his textbook, *Computer Security: Art and Science*, was published in 2002 by Addison-Wesley Professional. He is currently a co-director of the Computer Security Laboratory at the University of California Davis.



Marcelo Antonio Marotta is an assistant professor at University of Brasilia, Brasilia, DF, Brazil. He received his Ph.D. degree in Computer Science in 2019 from the Institute of Informatics (INF) of the Federal University of Rio Grande do Sul (UFRGS), Brazil. His research involves Heterogeneous Cloud Radio Access Networks, Internet of Things, Software Defined Radio, Cognitive Radio Networks, and Network Security.